CLEAR BAND FORMATION SIMULATED BY DISLOCATION DYNAMICS

Thomas Nogaret[1,2], David Rodney[1], Marc Fivel[1], Christian Robertson[2]

[1]SIMAP-GPM2, INP Grenoble, CNRS/UJF, BP46, 38402 Saint Martin d'Heres, France;

[2]SRMA, CEA DEN/DMN Saclay, 91191 Gif-Sur-Yvette, France

Dislocation Dynamics simulations of dislocations gliding across a random populations of Frank loops are presented. Specific local rules are developed to reproduce elementary interaction mechanisms obtained in Molecular Dynamics simulations. It is shown that absorption of Frank loops as helical turns on screw dislocations governs the process of clear band formation, because: (1) it transforms the loops into jogs on dislocations, (2) when the dislocations unpin, the jogs are transported along the dislocation lines, leading to a progressive clearing of the band and (3) the dislocations are re-emitted in a glide plane different from the initial one, allowing for a broadening of the band. It is also shown that a pile-up of dislocations is needed to form a clear band of finite thickness.

1. INTRODUCTION

Neutron irradiation causes a degradation of the mechanical properties of metals: a pronounced hardening, a reduction of ductility and plastic instabilities are observed [1]. In stainless steels, hardening is usually ascribed to the creation of a high density of nanometer-sized irradiation defect clusters, in the form of interstitial Frank Loops [2-4]. Ductility reduction and plastic instabilities are associated with the localization of the deformation into defect-free shear bands called clear bands [5, 6]. Clear bands are characterized by a constant thickness that depends on the resistance of the defects. Weaker defects, such as SFTs, lead to wider clear bands than stronger obstacles, such as Frank loops: □100 nm for the former compared to □20 nm for the latter [7]. The formation mechanism of clear bands remains however not well understood; namely, the clearing and broadening mechanisms of the bands are still unknown.

Recently, important modelling and experimental efforts have been devoted to investigate the elementary interaction mechanisms between dislocations and irradiations defects. Systematic studies were performed by Molecular Dynamics (MD) simulations [8, 9]. The interaction mechanisms with Frank loops and SFTs were found in strong analogy. In both cases, edge and screw dislocations behave differently. Screw dislocations mainly absorb defects as helical turns whereas edge dislocations shear the defects at low applied stresses. Screw dislocations are strongly pinned by helical turns because the latter can glide only in the screw direction. When screw dislocations unpin, they are reemitted in a glide plane parallel to the initial glide plane, because of the three-dimensional structure of the helical turn. Similar behaviors were observed in in-situ Transmission Electron Microscopy (TEM) [10]: screw dislocations are mainly responsible for defect removal, absorb defects as helical turns and are re-emitted in new glide planes upon unpinning. TEM observations showed also that clear bands are formed by screw dislocation pile-ups emitted from heterogeneities, such as grain boundaries [6]. Conventional Frank Read sources are indeed strongly pinned by the formation of dense clouds of defects during the irradiation [11] and remain inactive.

Nevertheless, the role of the above nano-scale interaction mechanisms in forming micron-scale clear bands has yet to be demonstrated. Dislocation Dynamics (DD) simulations are suitable for addressing this issue. In the early 2000's, DD simulations were performed in order to study clear band formation by dislocations generated from a Frank Read source and interacting with a population of irradiation defects [12-15]. However the local rules used to model the

short-range interactions between dislocations and irradiation defects were very simple: no distinction between screw and edge dislocation was made and the defects were systematically removed from the simulation cell, after interaction.

In this paper, an existing DD code is modified in order to accurately reproduce the MD interaction mechanisms. The different behaviors between screw and edge dislocations are reproduced with realism by using specific local rules of interaction and using an undecorated initial dislocation source, positioned at the simulation cell boundary. In Section 2, TEM observation of ion irradiated stainless steel specimens are first described. Information from these experiments are used in for the simulation settings to be described Section 3, where the simulation techniques are presented, i.e. the parameters and the configurations, the local rules of interaction and the elementary interaction mechanisms. In Section 4, the cases of isolated dislocation and collective dislocation interaction with a random population of defects are presented. In Section 5, the results are discussed with respect to experiments and previous simulations.

2. TEM OBSERVATION OF CLEAR BANDS IN ION IRRADIATED STAINLESS STEEL

Flat shaped tensile specimens were machined from solution annealed AISI 316L steel plates. The stacking fault energy (SFE) of this alloy is about 30 mJ/m^2, i.e. it is consistent with the interatomic potential used in the MD simulations to be described in the next section. Some specimens were irradiated at 350 °C using 2.1 MeV Kr ions, yielding a 0.5 µm thick irradiated surface layer, with peak damage around 3 dpa. Other specimens were irradiated at 350 °C using 95 MeV Xe ions, yielding a 10 µm thick irradiated surface layer with a mean irradiation dose around 1 dpa. All the specimens were then strained in uni-axial tension at 350 °C with a 10^{-4} s^{-1} strain rate up to 8% plastic strain then, finally thinned down to 100 µm by mechanically polishing the un-irradiated surface.

Then, 3 mm discs were punched out and TEM thin foils were obtained by a back-side electro-polishing technique.

The irradiation defects visible in the TEM samples are interstitial Frank loops with a diameter around 10 nm, i.e. the same defects and the same size as considered in the MD simulations. The loop density is about 10^{23} min^{-3} the 3 dpa irradiated samples, and about 10^{22} m^{-3} in the 1 dpa irradiated samples, also consistent with the MD simulation setting to be described in Section 3.

After plastic straining, clear bands of thickness 20-80 nm were observed in the 1 dpa irradiated samples. Two examples of clear bands are shown in Fig. 1: the two bands are located in the same grain and are parallel to 2 distinct {111} glide planes. The observed channel width in stainless steel is about one order of magnitude smaller than in irradiated Cu deformed at the same temperature [5]. It is believed that thinner channels are obtained in stainless steel because cross-slip is more difficult than in Cu, owing to the lower SFE of the steel ($SFE_{316L} < SFE_{Cu}$), at the same temperature[1]. It was indeed explained above that cross-slip is of prime importance for defect absorption, during MD simulations (see Section 3).

Dislocation lines present in the vicinity of the clear bands are shown in Fig. 2, at higher magnification. The dislocations are heavily jogged and appear wiggly in the micrographs. These line shapes are most probably due to the absorption of Frank loops and their transformation into jogs along the dislocation lines, as is observed in the MD simulations [9]. Information from the various micrographs provides insight regarding the clear band formation process.

In Fig. 3 two distinct and parallel clear bands are visible in the same grain. The width of the two clear bands is nevertheless quite different: one is rather wide and well developed while the other is much narrower.

[1] Conversely, the channel width in irradiated Cu at room temperature (and lower) is comparable (to within a factor 2) to the channel width observed in irradiated 316L steel deformed at 350 °C.

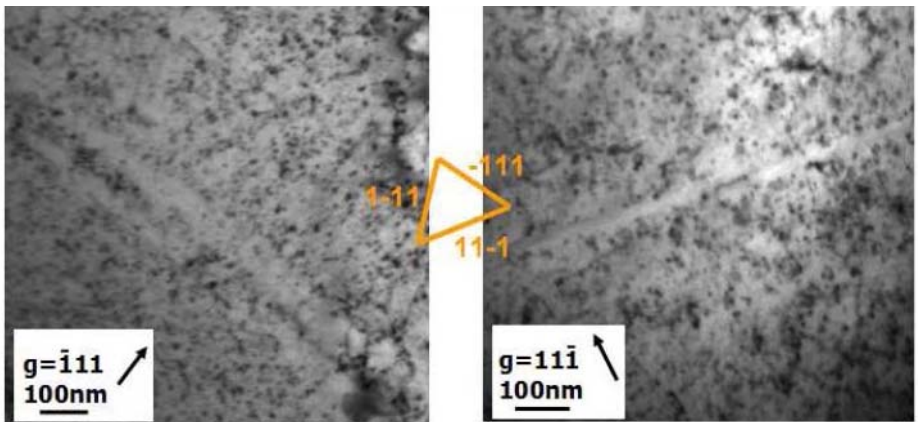

Fig. 1. Clear bands observed after deformation of samples irradiated to 1 dpa

a

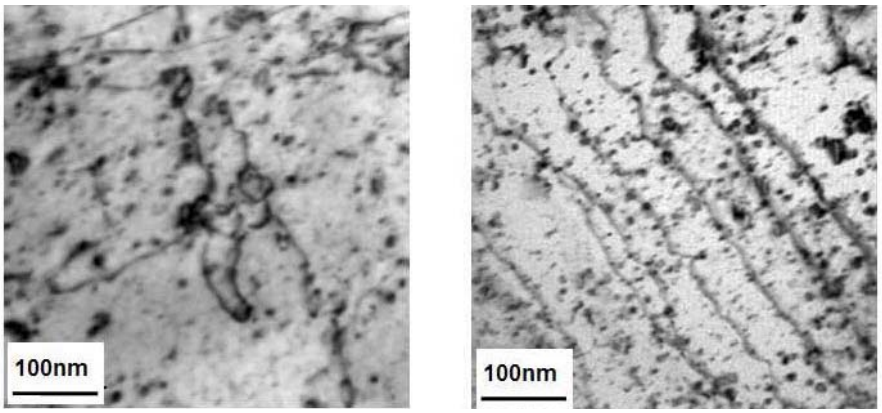

b

Fig. 2. Dislocations observed after deformation of samples irradiated to 1 dpa

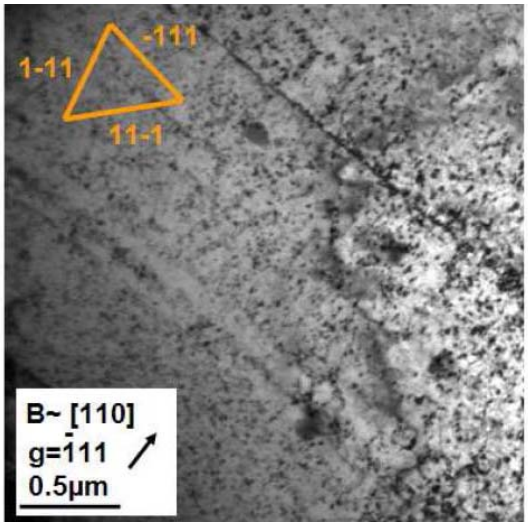

Fig. 3. Two clear bands observed in a same grain after deformation of samples irradiated to 1 dpa

In addition, no dislocation is visible in the wide clear band whereas a dislocation pile-up can be clearly seen in the narrow clear band. If the formation of a pile-up structure is interpreted as a prior step for clear band formation, the observations prove that the overall process is rather progressive and involves the passage of many dislocations. Analysis of the dislocations observed in clear bands show that they mostly adopt the screw character (see Fig. 2,a). These observations are consistent with in-situ TEM analyses [6] and with the scenario proposed from the MD simulations described in Section 3. Indeed, during the formation of a clear band, the first dislocations to glide in the band absorb many defects and become heavily jogged and wiggly, as illustrated in Fig. 4,b. If the applied

stress is removed during this first stage of clear band formation, the dislocations remain pinned in the band, because they are heavily jogged. Then, these dislocations are visible in post-mortem samples. By way of contrast, the dislocations that travel in a well formed clear band see hardly any defects. These dislocations therefore remain free of jogs and either glide back upon specimen unloading or are eliminated afterwards, during the TEM foil preparation. Well-developed clear bands therefore contain no dislocations in post-mortem observations.

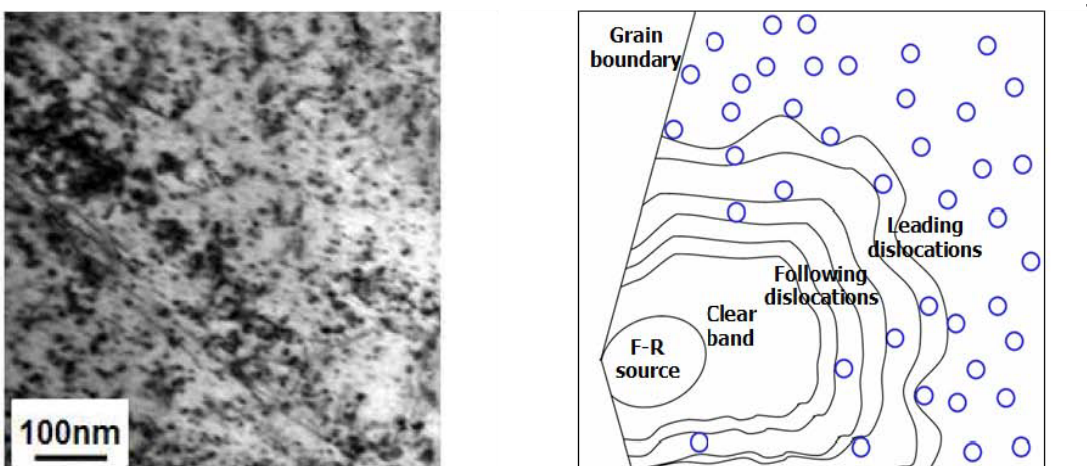

a b

Fig. 4. Pile-up of screw dislocations observed in a thin shear band (a), Simplified illustration of the progressive process of clear band formation (b)

In conclusion, clear bands and wiggled dislocations were observed in ion irradiated specimens, after tensile straining at 350 °C. Clear band formation is believed to be a progressive, three-dimensional process, involving numerous dislocation passages.

3. THE COMPUTATIONAL MODEL

3.1. The simulation cell

The Dislocation Dynamics code used in this work was first developed by Verdier et al. and is described in details in [16]. Only the points specific to the present study are addressed here. Dislocation lines are discretized in edge and screw segments that glide on a discrete lattice homothetic to the underlying crystallographic structure. The segments are treated as elastic inclusions, generating long-range stress fields included in the calculation of the local resolved shear stress, acting in the simulation volume. Usually, the parameter of the discrete lattice is 10b, where b is the magnitude of the Burgers vector. In the present work, in order to model nanometric defects and sub-nanometric jogs on dislocations, a smaller parameter 0.08b is used. Consequently, the time step has been reduced; down to $5 \cdot 10^{-14}$ s. Elasticity is isotropic and corresponds to a copper crystal in agreement with the MD simulations [9]. The adopted simulation cell is shown in Fig. 5. Its dimensions are 0.6x0.6x0.24 m. The borders act as impenetrable grain boundaries and cannot be crossed by the dislocations. Horizontal planes are Z = (111) glide planes, while the Y axis is along the [10-1] Burgers vector direction. In order to account for dislocation emission from heterogeneities as observed experimentally in irradiated materials [6,19], a dislocation source is placed along a border of the cell and model a grain boundary source. Different types of sources that emit either edge or screw dislocations were tested, as well as sources of different lengths (see Section 4.1). The applied stress tensor is composed of only the σ_{YZ} shear component which is feedback controlled in order to impose a constant strain-rate of $1.2 \cdot 10^{3}$ s^{-1}. It is worth recalling that no thermally-activated mechanisms (including cross-slip) are allowed in the presented simulations.

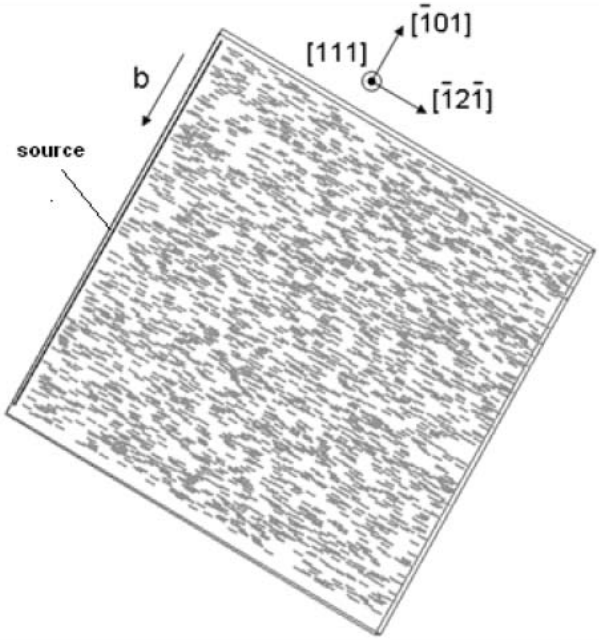

Fig. 5. Simulation cell. The loops are in grey, a screw dislocation appears in the upper left border

The adopted simulation method is therefore best adapted to analyse details of post-irradiation plastic deformation at rather low temperature (below creep threshold). This method cannot reproduce high temperature in-flux situations like irradiation creep; unless a specific dislocation climb treatment is implemented.

In absence of detailed knowledge on exactly how actual grain boundary sources operate, a simple emission criterion is used: the source emits a new dislocation when the applied stress σ_{YZ} reaches a critical value, called the nucleation stress τ_{nucl}. During a simulation, this stress is the maximum value that the applied stress may reach because in such a case, a dislocation is emitted, leading to an increment in plastic deformation that decreases the applied stress. The emitted dislocations belong to the .<10-1>{111} system, to be called the primary slip system. The cross-slip system is .<10-1>{1-11}. Both systems share the primary Burgers vector .<10-1>. The MD simulations show that when a Frank loop is unfaulted by interaction with a dislocation, it systematically obtains the Burgers vector of the incoming dislocation [9]. Thus, in order to keep a simple computational model, the Frank loops are modelled as interstitial prismatic loops with the primary .<10-1> Burgers vector. The initial loop shape is parallelepipedic, composed of 2 segments in the primary system and two segments in the cross-slip system. The length of all the fixed segments (and thus, the size of all the loops) is set to D = 10 nm, representative[2] of the irradiation conditions as described in Section 2. The loops are placed at random positions in the simulation cell, with a density $N=3.7\cdot10^{22}$ m^{-3}, in agreement with typical TEM observations in irradiated stainless steels (4). The associated mean inter-loop interval (projected in the glide planes) is then $L=1/\sqrt{(N\cdot D)}$ = 52 nm, which also corresponds to the distance adopted in MD simulations.

3.2. Elementary interaction mechanisms

Frank loops are sessile because they contain a stacking fault. Such loops are unfaulted and become glissile through the interaction with screw dislocations, while they remain faulted and are simply sheared when interacting with edge dislocations. In order to reproduce these elementary interactions, the loops in the simulation cell are initially frozen, i.e. their segments are immobile. When a dislocation comes in contact with a loop, its character is identified by computing the angle between the local tangent to the dislocation line and the Burgers vector. If this angle is $\pm20^{\circ}$, the dislocation is declared screw and the loop segments are "freed", i.e. they are allowed to move according to the forces acting on them. As will be seen in next paragraph, a helical

[2] The adopted simulation volume dimensions fix the maximum loop size that can be modeled. The simulation volume must be large enough to contain the loops and to accommodate the dislocation/loop reaction mechanisms as shown in fig. 6. With the simulation volume used here, D_{max} should be close to 50 nm.

turn then forms spontaneously. If the dislocation is not screw, the loop remains frozen and the contacting dislocation segments do not react with the loop. The dislocation is allowed to cross the loop when its arms on both sides of the loop reach a critical angle that was set to 100^{o} in order to match the resistance obtained in MD simulations, i.e. a critical shear stress of 130 MPa for an inter-loop distance of 50 nm [9].

The interaction between a screw dislocation and Frank loops is sketched in Fig. 6. The incoming screw dislocation contacts a Frank loop. At this moment, the segments forming the loop are freed. They react with the dislocation and spontaneously form a helical turn (Fig. 6,b), made of 20 nm long segments: 3 super-jogs in (1-11) cross-slip planes and 2 segments in (111) primary planes located above and below the initial glide plane. The initial dislocation thus ends up with a 3D structure. It does not belong to the initial glide plane anymore because the helical turns expanded along the dislocation line in order to minimize the dislocation length and the associated line tension energy.

The dislocation is pinned by the helical turns because the super-jogs in cross-slip planes can glide only in the [10-1] direction of the Burgers vector, i.e. along the dislocation line, and not in the initial [-12-1] glide direction. Dislocation unpinning requires the activation of a 20 nm long super-jog in a (111) glide plane (Fig. 6,d). The activated segment belongs to a (111) plane located above (along the [111] direction) the initial glide plane. Indeed, it can be shown from a line tension approximation of a helical turn that upon increasing shear stress, the segment located furthest in the glide direction becomes unstable first. Consequently, a dislocation that glides in the [-12-1] (resp. [1-21]) direction is re-emitted in an upper (resp. lower) (111) plane. In the following, it is shown that this unpinning mechanism plays a central role in clear band broadening, as will be demonstrated next.

The interaction between an edge dislocation and three Frank loops is depicted in Fig. 7. As a stress is applied, the mobile edge dislocation bows out and comes into contact with one of the loops (Fig. 7,a). The dislocation is then blocked and bows out. When the applied stress reaches 130 MPa, the angle between the dislocation arms pinned on the central loop reaches the critical angle of 100° (Fig. 7,b) and the dislocation is allowed to go through the loop. The latter remains frozen and is left unchanged, since it was observed in MD simulations that the step created on the loop is mobile and annihilates on the loop border, thus reforming the initial loop configuration.

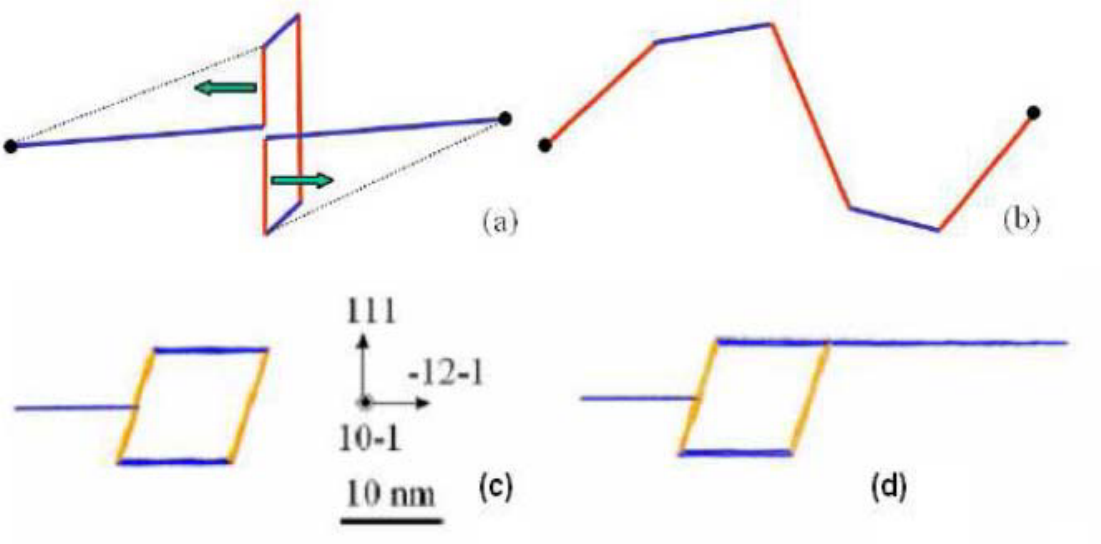

Fig. 6. Interaction between a screw dislocation and Frank loop.
The dislocation glides in a (111) plane and comes into contact with the loop in its middle (a); absorbs the loop as a helical turn (b). The same reaction as in (a) is shown in (c), from a different viewing angle. In (d), it is clearly seen that a dislocation segment located in an upper (111) plane is activated at the time of unpinning from the helical turn

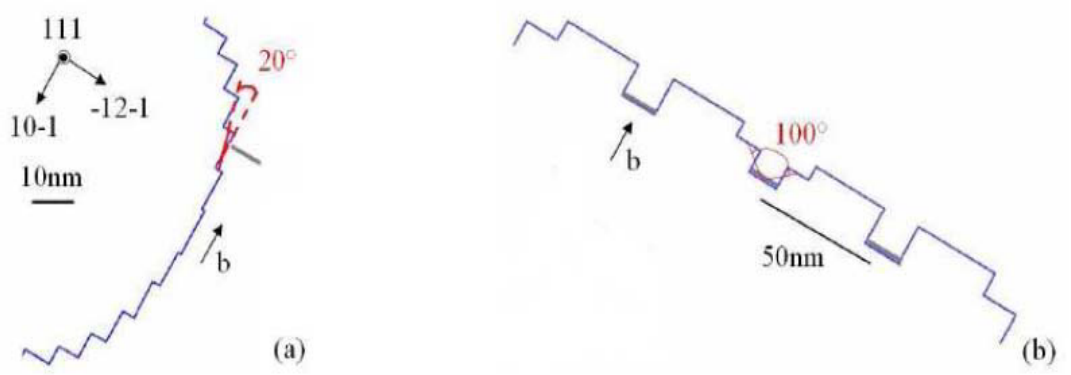

Fig. 7. Interaction between an edge dislocation and a Frank loop. An edge character dislocation glides towards an immobile Frank loop (a). The incoming dislocation is blocked and bows out until the critical bowing angle of 100° is reached on the loop (b). The sheared loop remains "frozen" after the mobile dislocation unpins, i.e. it stays at the same initial location as before the interaction

4. GLIDE IN RANDOM LOOP ENVIRONMENTS

In this section, the glide of dislocation(s) through a random population of Frank loops is simulated. Two glide regimes are studied by changing the magnitude of the nucleation stress τnuc. The case where the nucleation stress is much larger than the loop resistance is first evaluated, in Section 4.1. A single dislocation then glides through the simulation cell, driven by the applied stress only. In the second case, treated in Section 4.2, the nucleation stress is lower than the loop resistance and so, no isolated dislocation can glide on its own. More dislocations are then nucleated until a pile-up is formed, leading to collective interaction effects, that enable the dislocations to glide through the cell at an applied stress lower than when isolated.

4.1. Glide of single dislocations

A nucleation stress of 1000 MPa is used, i.e. much larger than the loop resistance evaluated in Section 3.2 (in MD simulations, for instance). The applied stress needed to accommodate the imposed plastic strain rate is always lower than the nucleation stress and only one dislocation glides through the cell. Dislocation sources emitting 200 nm long dislocations of either edge or screw characters are tested. Let's consider first the case of an edge source, as shown in Fig. 8. In Fig. 8, a which shows a [111] top view of the simulation cell, the edge part emitted from the source glides mainly by shearing loops. It produces on its sides two long dislocations of screw character. The latter are wavy and composed of segments in the primary glide plane as well as in cross-slip planes.

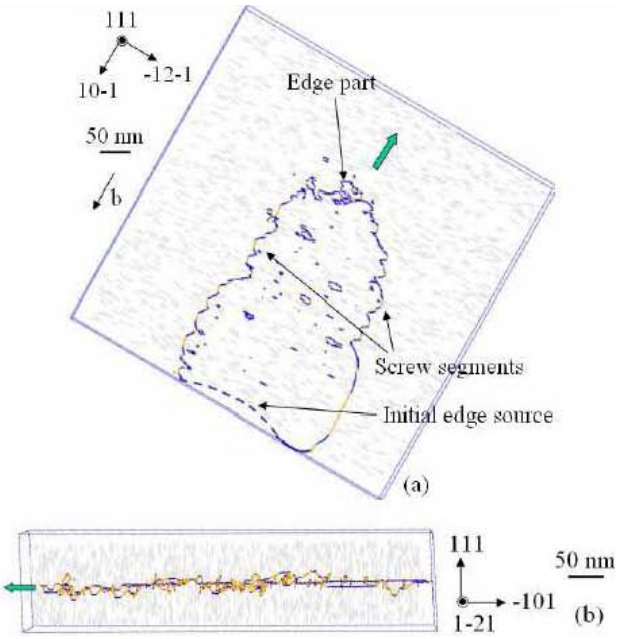

Fig. 8. Gride of a single edge dislocation: a – [111] top view (untouched loops are in ligt grey, segments in (111) planes in blue, segments in cross-slip planes in orange; b – stress/strain curve; c – [1-21] side view (the green arrow shows the direction of glide)

These segments form helical turns created on the dislocation line by the unfaulting and absorption of Frank loops, following the same interaction mechanism as described in Section

3.2. While the edge segment is mobile, the two screw dislocations are strongly pinned. The [1-21] side view of Fig. 8, b shows that dislocation glide is planar on average, although segments in cross slip planes (belonging to helical turns), are also visible. The accompanying stress/strain curve (not shown) reveals that the stress required for the glide of a single edge dislocation is between 130 and 160 MPa, depending on the local loop density met by the dislocation along its path.

The screw case is shown in Fig. 9. As the screw dislocation emitted from the source advances through the simulation cell, it creates edge parts that glide easily until they reach the cell borders, while the screw segment unfaults and absorbs loops as helical turns (see Fig. 9, a). The dislocation soon adopts the shape of a long screw segment that traverses the whole cell in the [10-1] direction, with edge segments stacked on the cell boundaries. Thus, edge and screw sources lead to similar microstructures made of screw dislocations that extend over the entire length of the simulation cell.

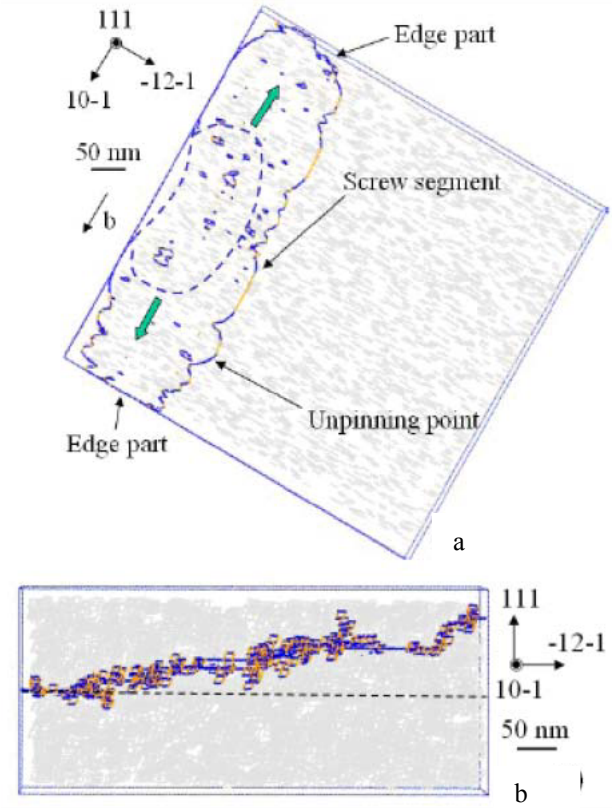

Fig. 9. Glide of a single screw dislocation : a – [111] top view; b – stress/strain curve

Using a screw type source, the stress required for dislocation glide is between 200 and 260 MPa. The screw dislocation advances through the simulation cell by a mechanism close to the elementary mechanism described in Section 3.2: a succession of formation of helical turns that pin the dislocation followed by the activation of segments in the weakest zones along the dislocation, i.e. the zones where the jog density is the lowest. The activated segments glide on about 100 nm before being pinned again by helical turns. During this process, edge segments are created and glide easily towards the simulation cell borders. The edge segments, while travelling towards the cell borders, sweep the dislocation line and push the jogs on a finite distance towards the cell borders. This mechanism allows for a partial and progressive clearing of the swept zone.

As in the elementary reactions, when the screw dislocation unpins, it is systematically re-emitted in an upper (111) plane. Consequently, as seen in the [10-1] side view in Fig. 9, b, the dislocation glides in an average non-crystallographic plane, inclined with respect to the initial (111) plane, in contradiction with experimental observations. Moreover, no clearing is observed in Fig. 9, b. Plasticity is thus limited by screw dislocations and both edge and screw dislocation sources lead to the same anisotropic microstructure with strongly pinned screw segments that extend over the entire length of the simulation cell. Thus in the following, only the case of a screw dislocation source with a length equal to that of the simulation cell will be examined.

4.2. Collective dislocation motion

Now, in contrast with previous simulations, a low nucleation stress of 90 MPa is considered, i.e. below the critical stress for edge or screw dislocation glide. Consequently, a single dislocation cannot glide alone, and collective effects are needed to keep on deforming the simulation cell at the prescribed strain rate. Fig. 10 illustrates the obtained glide mechanism. The first dislocation nucleated acquires helical turns and becomes pinned. The stress in the simulation cell increases and reaches the nucleation stress, as shown by an arrow in Fig. 10, b. A second dislocation is then nucleated. It produces some plastic strain,

allowing the applied stress to drop. This second dislocation gets pinned as well, and the applied stress rises again, triggering the nucleation of a third dislocation, materialized by an additional arrow in Fig. 10,b.

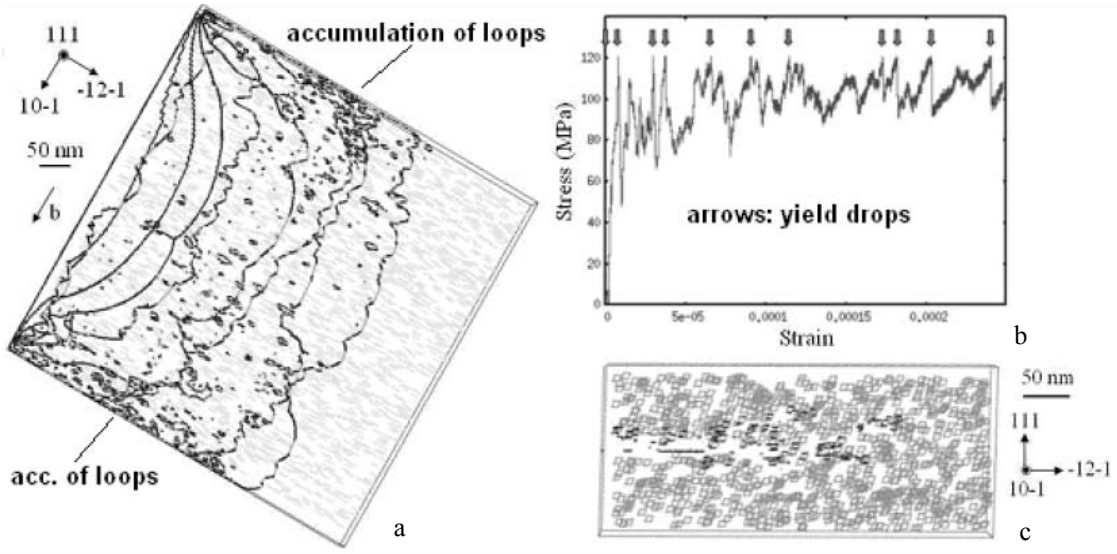

Fig. 10. Glide of a dislocation pile-up: a – [111] top view; b – stress/strain curve; c – [10-1] side view on a 200 nm thick thin foil

Dislocation pile-ups, as the one clearly visible in Fig. 10, a, thus form progressively. In this case, the 4 leading dislocations are wavy and heavily jogged. They are responsible for clearing the band by forming helical turns and pushing the jogs towards the cell borders upon unpinning. Accumulation of jogs is visible on the cell periphery in Fig. 10, a. Trailing dislocations contain very few jogs because they glide in the region cleared by the leading dislocations. The role of the trailing dislocations is to produce the pile-up effect and to concentrate the stress on the leading dislocations. Some heavily jogged dislocations are left behind, as seen in Fig. 10, a. They will presumably remain in the clear band. As in previous Section, the leading dislocations unpin in upper (111) planes and remain pushed by the pileup effect as long as they are not too far away from the initial central glide plane. As a consequence, as seen in Fig. 10, c, a cleared region of finite thickness develops parallel to the central (111) glide plane, in agreement with experiments. The pile-ups keep on advancing in the cell thanks to collective effects that include a stress concentration due to the pile-up effect, short range interaction mechanisms (arm exchange) and avalanches of dislocation glide. These interactions are described in detail in [20].

5. DISCUSSION

For the present study, Dislocation Dynamics simulations were adapted to the nanometer scale, in order to reproduce with realism the elementary interaction mechanisms observed in MD simulations. As a result, the computation load becomes very large and only the first stage of the clear band formation was simulated in a small grain (see Fig. 10, c). However, this study allows us to draw some conclusions about the mechanisms controlling the whole process.

The simulations confirm earlier MD results on the central role played by helical turns in clear band formation. Screw dislocations transform Frank loops into helical turns. The helical turns are then transported along the dislocation lines when they unpin leading to a progressive clearing of the band and to the accumulation of jogs and prismatic loops aligned in the edge direction. These loops have the same Burgers vector as the emitted dislocations, i.e. the primary Burgers vector. Helical turns are also central to clear band widening because upon unpinning, screw dislocations are re-emitted in new glide planes. This is equivalent to a double cross-slip over a height set by the loop size. This mechanism is consistent with the work of Neuhauser and Rodloff [19] who observed on the surface of

irradiated and deformed copper a distance between slip lines on the order to the defect size. Note that all the effects observed in the simulations were obtained while thermally-activated cross-slip and climb were switched-off. Hence, thermal activation is not a necessary condition for clear band formation. The microstructure obtained in the simulations, composed of long screw dislocations with accumulations of jogs and prismatic loops on the sides, is consistent with the TEM observations made by Sharp [5] who reported inside clear bands the presence of dense clusters of heavily jogged prismatic loops with a low density of screw dislocations, all sharing the same Burgers vector. To our knowledge, Sharp's work is the only case where a thin foil was prepared parallel to a clear band, making possible a detailed analysis of the microstructure inside a clear band. All other TEM studies of clear bands in irradiated materials used thin foils perpendicular to the clear band, which is the best orientation to locate a clear band, but the worst to study the microstructure inside the band.

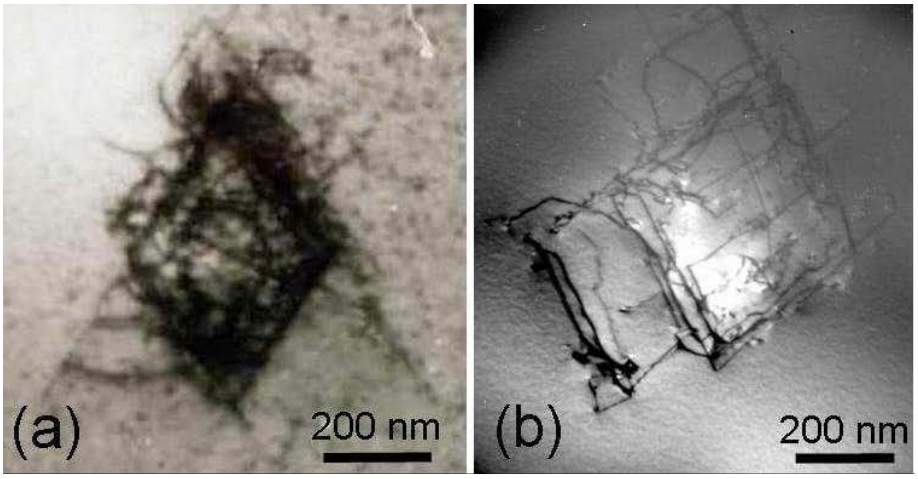

Fig. 11. Dislocation sources emitted at the tip of a nano-indenter in austenitic stainless steel. Irradiated 316L stainless steel, using 700 keV Kr^{3+} ions at 300 °C, 3 dpa (a). Non irradiated 316L steel (b). The indenter penetration depth is 30 nm in both cases

The present work shows the central role played by dislocation pile-ups. Hence, isolated dislocations can not form clear bands because band clearing is very progressive. In addition, isolated screw dislocations glide on non-crystallographic planes, owing to their systematic re-emission in upper (111) planes (see Fig. 10, c). In contrast, when dislocations glide in pileups, they remain along the central (111) plane (see Fig. 10, c) and generate stress concentration that contribute to re-activate (temporarily locked) dislocation arms located into different, parallel glide planes[3]. That is the reason why clear of finite thickness only form in presence of dislocations pile-ups. Sources of dislocations at the origin of clear bands must therefore emit a large number of dislocations. Since the sources prior to the irradiation are locked by decoration, the most probable sources are grain boundaries or other stress concentrators, such as inclusions (21) or singularities at grain boundaries. Note that hardening is not described in the present simulations because the resistance of the initial source, which controls the flow stress, is given as preset parameter. Clearly, more atomistic information is needed to better understand how heterogeneities may act as dislocation sources. Insight about the formation sources can also be obtained the other way around, by using TEM observation of dislocation emission from heterogeneous stress fields, in ion-irradiated materials (see Fig. 11 and [22]). In absence of this knowledge, a very simplified criterion was used in the present DD simulations.

The mechanisms controlling the width of clear bands have not been examined in details, owing to the computational load of the

[3] Stress concentration can be computed using analytical solutions or numerically, by adding the stress fields coming from selected dislocations (see Section 3).

simulations. However, one possible origin is the decay of the stress concentration away from the plane of the pile-up. Indeed, the leading dislocations of the pile-ups are heavily jogged and need a stress concentration to advance in the cell. As illustrated in Fig. 12, the stress on the dislocations ($\tau_{dislocation}$) is the sum of the applied stress ($\tau_{applied}$) and the stress concentrated by the pile-up ($\tau_{pile-up}$). The former is constant inside the simulation cell while the latter decreases away from the plane of the pile-up. When the leading dislocations unpin and are re-emitted in upper glide planes, they are subjected to a decreasing stress. There is thus a critical distance from the pile-up plane, which sets the band thickness, where the stress on the dislocations just balances the resistance due to the helical turns ($\tau_{unpinning}$) and the dislocations stop.

In their displacement, the leading dislocations have started to clear the band and the trailing dislocations can move forward and they eventually glide away from the plane of the pile-up until they are stopped and so on.

This scenario predicts that heavily jogged screw dislocations should be left in one side of the clear band (in this case, the upper glide plane). Although such arrays of screw dislocations have been observed [6], more TEM studies are needed. The present scenario also explains the experimental observation that the band width decreases when the resistance of defects or the resolved shear stress [7] or the defect density [5] increase.

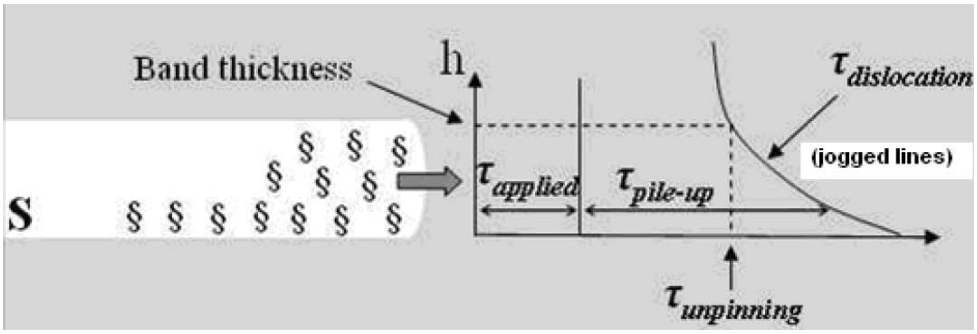

Fig. 12. Schematic representation of the equilibrium between the stress on the dislocations $\tau_{dislocation}$ (equal to the sum of the applied stress $\tau_{applied}$ and the pile-up stress concentration $\tau_{pile-up}$ and the defect resistance $\tau_{unpinning}$, which likely controls the band thickness

Indeed, for a given size of pile-up, the band width decreases if $\tau_{unpinning}$ increases, i.e. if the defects are intrinsically stronger or if they are in higher density; it also decreases if the resolved shear stress ($\tau_{applied}$) decreases.

6. CONCLUSION

The present work concludes a multiscale simulation study of the formation of clear bands. An existing DD code was modified to reproduce accurately MD results on elementary interaction mechanisms at the nanometer scale. The DD simulations in random loop environments confirm the central role played by helical turns in the formation of clear bands. It also shows that clear bands can not form without dislocation pile-ups. From the simulations, it is predicted that well-developed clear bands should contain heavily jogged screw dislocations as well as dense concentrations of prismatic loops. In order to confirm these predictions, detailed TEM analysis of the dislocation microstructure inside clear bands is needed.

This work was funded by the European PERFECT project (No. FI60-CT-2003-508840).

REFERENCES

1. K. Farrell, T. Byun, N. Hashimoto // *J. Nuc. Mat.* 2004, v. 335, p. 471–486.

2. M. Suzuki, A. Sato, N. Nagakawa, H. Shiraishi // *Phil. Mag.* 1992, v. A65, p. 1309–1326.

3. Y. Dai, X. Jia, J. Chen, W. Sommer, M. Victoria, G. Bauer // *J. Nucl. Mat.* 2001, v. 296, p. 174–182.

4. C. Pokor, Y. Brechet, P. Dubuisson, J. Massoud, A. Barbu // *J. Nuc. Mat.* 2004, v. 326, p. 19–29.

5. J. Sharp // *Phil. Mag.* 1967, v. 16, p. 77–96.

6. J. Robach, I. Robertson, A. Arsenlis //

Phil. Mag. 2003, v. 83, p. 955.
7. N. Hashimoto, T. Byun, K. Farrell // *J. Nucl. Mat.* 2006, v. 351, p. 295–302.
8. Y. Osetsky, D. Rodney, D. Bacon // *Phil. Mag.* 2006, v. 86, p. 2295–313.
9. T. Nogaret, C. Robertson, D. Rodney // *Phil. Mag.* 2007, v. 87(6), p. 945–66.
10. Y. Mastukawa, Y. Osetsky, R. Stoller, S. Zinkle // *Phil. Mag.* 2008, v. 88, p. 581.
11. B. Singh, A. Foreman, H. Trinkaus // *J. Nucl. Mat.* 1997, v. 249, p. 103.
12. T. delaRubia, H. Zbib, T. Khraishi, B. Wirth, M. Victoria, M. Caturla // *Nature.* 2000, v. 406, p. 871–874.
13. N. Ghoniem, S. Tong, B. Singh, L. Sun // *Phil. Mag.* 2001, v. A 81, p. 2743–64.
14. T. Khraishi, H. Zbib, T. de la Rubia, M. Victoria // *Met. Mat. Trans.* 2002, v. B 33, p. 285–296.
15. N. Ghoniem, S. Tong, J. Huang, B. Singh, M. Wen // *J. Nucl. Mat.* 2002, v. 307-311, p. 843– 851.
16. M. Verdier, M. Fivel, I. Groma // *Mod. Sim. Mat. Sc. Eng.* 1998, v. 6, p. 755–70.
17. J.P. Hirth, J. Lothe. *Theory of Dislocations.* Krieger, Malabar, 1992.
18. T. Khraishi, H. Zbib // *Phil. Mag. Let.* 2002, v. 82, p. 265–77.
19. H. Neuhauser, R. Rodloff // *Acta Met.* 1974, v. 22, p. 375.
20. Nogaret // *JNM*, 2008
21. D. Edwards, B. Singh, J. Bilde-Sorensen // *J. Nucl. Mat.* 2005, v. 342, p. 164–78.
22. Communication SMORE meeting.

МОДЕЛИРОВАНИЕ МЕТОДАМИ ДИСЛОКАЦИОННОЙ ДИНАМИКИ ОБРАЗОВАНИЯ СВОБОДНЫХ ЗОН

Томас Ногарет, Дэвид Родни, Марк Файвел, Кристиан Робертсон

В терминах дислокационной динамики представлено моделирование дислокаций, пересекающих расположенную случайным образом совокупность петель Франка. Разработаны локальные правила для воспроизведения элементарных механизмов взаимодействия, полученных при моделировании методом молекулярной динамики. Показано, что поглощение петель Франка в виде геликоидальных витков на винтовых дислокациях определяет процесс образования свободных зон, поскольку: 1) оно преобразует петли в ступеньки на дислокациях, 2) в случае открепления дислокации ступеньки переносятся вдоль линий дислокаций и 3) дислокации вновь поступают в плоскость скольжения, отличающуюся от исходной, обеспечивая тем самым расширение свободной зоны. Кроме того, показано, что скопление дислокаций необходимо для образования свободной зоны с конечной толщиной.

МОДЕЛЮВАННЯ МЕТОДАМИ ДИСЛОКАЦІЙНОЇ ДИНАМІКИ УТВОРЕННЯ ВІЛЬНИХ ЗОН

Томас Ногарет, Девід Родні, Марк Файвел, Крістіан Робертсон

У термінах дислокаційної динаміки представлено моделювання дислокацій, що перетинають розташовану випадковим чином сукупність петель Франка. Розроблені локальні правила для відтворення елементарних механізмів взаємодії, що отримані при моделюванні методом молекулярної динаміки. Показано, що поглинання петель Франка у вигляді гелікоїдальних витків на гвинтових дислокаціях визначає процес утворення вільних зон, оскільки: 1) воно перетворює петлі у східці на дислокаціях, 2) у випадку відкріплення дислокації східці переносяться вздовж ліній дислокацій і 3) дислокації знову надходять у площину ковзання, яка відрізняється від вихідної, забезпечуючи тим самим розширення вільної зони. Крім того, показано, що скупчення дислокацій необхідне для утворення вільної зони з кінцевою товщиною.